Precipitation of Carbides in 12% Cr Steel during Tempering*

Tsuyoshi MASUMOTO, Shigeru TAKEDA and Yûnoshin IMAI

The Research Institute for Iron, Steel and Other Metals

(Received April 7, 1970)

Synopsis

Precipitation characteristics of 12% Cr steel during isothermal tempering were studied mainly by transmission electron microscope. As the result, the shape, nucleation site and habit plane of each carbide (Fe_3C, $(Cr, Fe)_7C_3$, $(Cr, Fe)_{23}C_6$), and the orientation relationships between carbides and ferrite matrix were clarified. It was confirmed that the transformation of Fe_3C into $(Cr, Fe)_7C_3$ occurred by both *in situ* and separate nucleation, and that of $(Cr,Fe)_7C_3$ into $(Cr,Fe)_{23}C_6$ by separate nucleation on grain boundaries. Furthermore, it was concluded that the secondary hardening might be induced by the distribution of fine granular particles of $(Cr, Fe)_7C_3$ nucleated separately on the dislocations in the region of high dislocation density.

I. Introduction

Studies on the precipitation process of 12% Cr steel during tempering are important, because this steel is used in the state of secondary hardening through processes of quenching and tempering. Hitherto, the carbide reaction such as $\varepsilon \rightarrow Fe_3C \rightarrow (Cr, Fe)_7C_3 \rightarrow (Cr, Fe)_{23}C_6$ has been observed on tempering by means of dilatation, electric resistance, magnetic analysis, X-ray diffraction, extracted replica and extracted residue methods.[1),2)] In spite of a large number of researches, however, precipitation behaviors of each kind of carbides have not been fully explained because of indirect methods of observation. The aim of the present work was to make clear the precipitation site, transformation mechanism (*in situ* or separate nucleation) of carbides, and their orientation relationships to matrix, and further, the relation of precipitation behavior to secondary hardening.

II. Experimental procedure

Alloys were prepared by melting suitable mixtures of electrolytic pure iron, electrolytic chromium and high purity iron-carbon alloy in a high induction vacuum furnace. The as-cast alloys were hot- and cold-rolled into rods 6 mm in dia. From these rods, specimens were prepared for chemical analysis, and for tests of hardness ($5\phi \times 7$ mm) and compression ($5\phi \times 5$ mm), and also thin sheets (0.12 mm) were pre-

* The **1453rd** report of the Research Institute for Iron, Steel and Other Metals. Published in Japanese in the J. of Japan Inst. Metals, **33** (1969), 1024.

(1) T. Sato et al., J. Japan Inst. Metals, **22** (1958), 484.

(2) J. Koutsky et al., Hutnické Listy, **13** (1958), 12.

Table 1. Chemical composition of specimen

Element	C	Si	Mn	Cr	N	Fe
wt %	0.16	0.02	<0.01	12.28	0.004	Bal

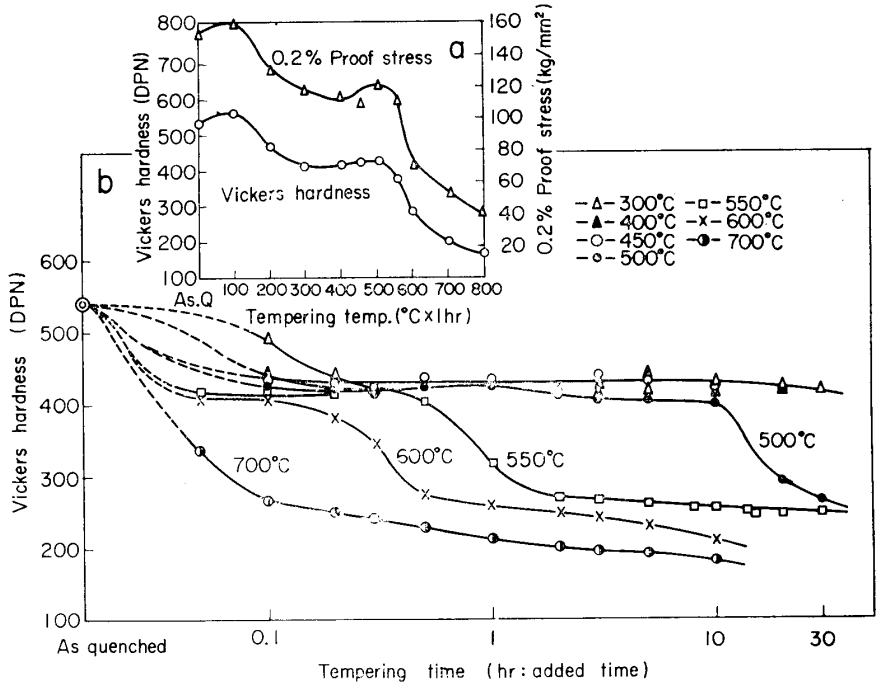

Fig. 1. (a) Isochronal curves of hardness and 0.2% proof stress during tempering.
(b) Isothermal curves of hardness at various tempering temperatures.

pared for electron microscopic observation. Table 1 shows chemical composition of the specimen.

Specimens were homogenized at 1300°C for 1 hr, quenched in water, sub-zero treated in liquified nitrogen (D.P. about -180°C) to decompose residual austenite fully and then tempered. All heat treatments were carried out in sealed silica capsule in vacuum.

For strength tests, Vickers hardness and 0.2% proof stress in compression using Instron were measured.

Thin foils were obtained from these heat-treated sheets by Jet method and subsequently by improved Bollmann method both by using perchloric acid — methyl-alcohol solution as electrolyte, and then were examined by means of a Hitachi HU-10 electron microscope at 100 kV.

III. Experimental results and discussions

1. Electron microscopy

In reference to the age-hardening character of the specimen steel, Fig. 1(a) shows the changes in isothermal hardness and 0.2% proof stress during one-hour tempering at various temperatures ranging over 100～800°C, and Fig. 1(b) the

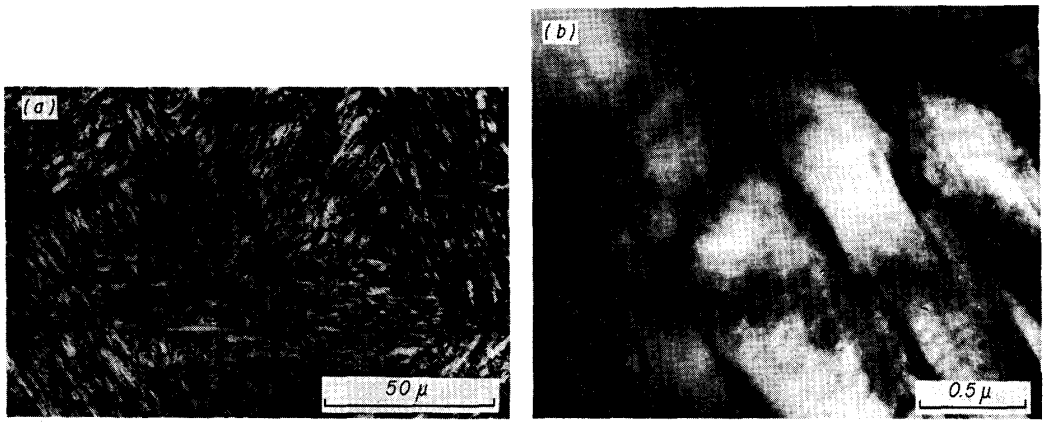

Photo. 1. Microstructures of specimen quenched from 1300°C.
(a) by optical microscope (b) by transmission electron microscope

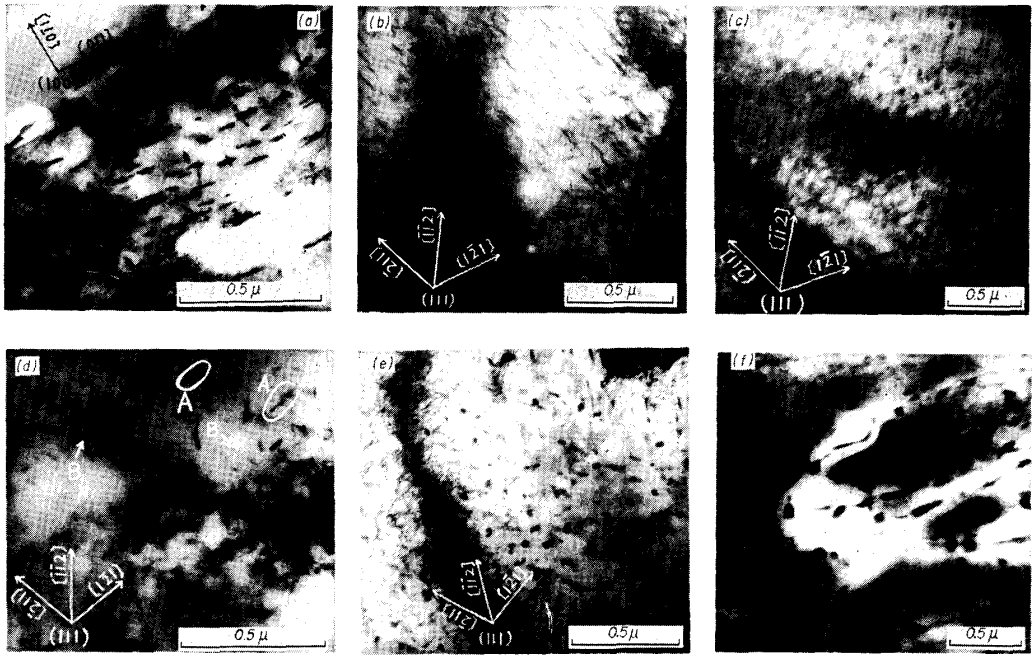

Photo. 2. Transmission electron micrographs of 12%Cr–0.16%C-Fe steel
(a) tempered at 550°C for 5 min (b), (c) tempered at 550°C for 20 min (d) tempered at 550°C for 1 hr (e) tempered at 550°C for 8 hr (f) tempered at 550°C for 100 hr

changes in isothermal hardness in the range of 300～700°C (tempering time being prolonged). Fig. 1(a), beside the hardening caused by ε- carbide precipitation around 100°C, shows clearly the secondary hardening in the neighbourhood of 500°C. On the other hand, in Fig. 1(b), of the curves displaying two-stage softening, those for 500°C and 550°C show the secondary hardening, though slight in degree, following the first-stage softening. For instance, in the tempering at 550°C, the first-stage softening finishes in about 5 min, and the secondary hardening occurs at the prolonged time of some 20～30 min, and then the second-stage softening suddenly sets in to follow a decline.

On this account, some examinations were carried out on the precipitation structure when isothermally tempered at 550°C, in which secondary hardening clearly occurs.

In the quenched specimen, the structure is homogeneous martensite as shown in Photo. 1(a) (by optical microscope) and is massive as shown in Photo. 1(b) (by transmission electron microscope).

Photos. 2(a)~(f) show the typical examples of structures tempered for 5 min to 100 hr at 550°C. Photo. 2(a) shows the structure of the steel tempered for 5 min, in which the first-stage softening appears. As shown in Photo. 2(a), needle-like precipitates (about 1000 Å in length) nucleate, with fixed orientation, within the grain. By the analysis of electron diffraction, these precipitates were identified as Fe_3C, and were analyzed to grow in the <110> direction of matrix. Photos. 2(b) and 2(c) show the structures in the stage of 20 min tempering, where, in addition to the needle-like Fe_3C just as seen in the structure in the stage of tempering for 5 min (b), granular particles (about 150~200 Å in length) are shown as have nucleated on the dislocations in the region of high dislocation density (c). These two types of precipitate are supposed to be different in kind, because in Photos. 2(b) and 2(c), both are the same with (111) reflections. In this regard, dark field reflection method was employed to make the above results sure.

Photo. 3(a) shows a bright field image, in which both precipitates in question coexist, and 3(b) a dark field image taken with the diffraction spot of particles except Fe_3C. These instances suggest that this granular particle is newly nucleated. As to the specimen tempered for 30 min and that for 40 min, the structures were found to be the same as that tempered for 20 min. The habit plane of the needle-like Fe_3C was analyzed by stereography to be {110} ferrite plane.

Photo. 2(d) shows the structure of the specimen tempered for 1 hr, in which the hardness suddenly decreases more sharply than before. In this structure, both Fe_3C and $(Cr,Fe)_7C_3$ were identified by means of electron diffraction pattern. As shown in Photo. 2(d), a needle-like precipitate splits into several parts, encircled region marked as A and in another place marked as B, small-granular precipitates are observed.

According to the dark field image, granular precipitates in region B are $(Cr, Fe)_7C_3$, and the split of the needle-like precipitate is supposed to be the result of transformation of Fe_3C into $(Cr, Fe)_7C_3$. Further in the specimen tempered for a few hours, Fe_3C disappears and only $(Cr, Fe)_7C_3$ exists. After that, besides $(Cr, Fe)_7C_3$ which has the same growth direction as Fe_3C, granular $(Cr, Fe)_7C_3$ grows in the specimen tempered for 8 hr. In the specimen tempered for 12 hr, massive precipitates nucleate newly on sub-boundary and grain boundary with a decrease of ganular and needle-like precipitates within the grain.

Photo. 4, showing dark field image operated by $(333)_{(Cr,Fe)_{23}C_6}$ reflection, indicates that these precipitates on grain boundary are $(Cr, Fe)_{23}C_6$. Evidence

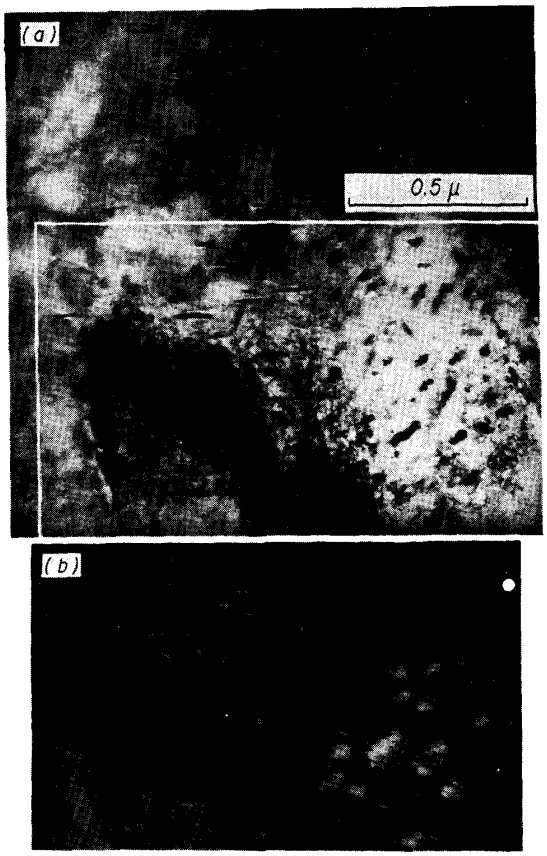

Photo. 3. Electron micrographs showing types of carbides precipitated within a grain in specimen tempered at 550°C for 20 min.
(a) Bright field image. (b) Dark field image.

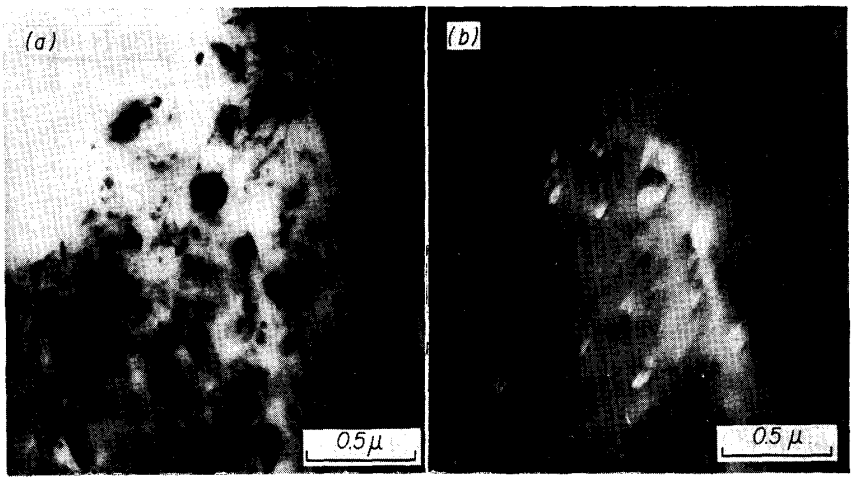

Photo. 4. Electron micrographs showing precipitation of $(Cr, Fe)_{23}C_6$ at grain boundary in 12% Cr steel tempered at 550°C for 20 hr.
(a) Bright field image (b) Dark field image by $(333)_{Cr_{23}C_6}$ reflection operating.

that the transformation of (Cr, Fe)$_7$C$_3$ into (Cr, Fe)$_{23}$C$_6$ occurs *in situ* was not obtained, and it is considered as separate nucleation on subgrain boundary. The precipitates on grain boundary grow gradually with the increase in tempering time, and (Cr, Fe)$_7$C$_3$ dissolves. For example, as shown in Photo. 2(f), in the specimen tempered for 100 hr, (Cr, Fe)$_7$C$_3$ within the grain is few and (Cr, Fe)$_{23}$C$_6$ grows largely on grain boundary.

According to the reports in the past, the transformation process of each carbide is explained by replica method as follows: Fe$_3$C into (Cr, Fe)$_7$C$_3$ transformation occurs *in situ*,[3],[4] because the size and the distribution of carbides are not remarkably different before and after the transformation in Cr steel containing less than 9% Cr. But the proportion of separate nucleation to *in situ* transformation of Fe$_3$C into (Cr, Fe)$_7$C$_3$ increases with increasing carbon content in high Cr steel containing more than 9% Cr.[5]~[9] Many studies[7]~[11] favor that (Cr, Fe)$_7$C$_3$ into (Cr, Fe)$_{23}$C$_6$ transformation during last-stage tempering in Cr steel occurs *in situ*, but a recent reprot[12] insists on the separate nucleation.

In the present study, it is explained as follows:

Fe$_3$C nucleates homogeneously in the matrix with $\{110\}_\alpha$ habit plane, and grows needle-like in the direction $<111>_\alpha$. Next, (Cr, Fe)$_7$C$_3$ nucleates on the dislocations in the region of high dislocation density in separate nucleation, and Fe$_3$C within the grain dissolves to form (Cr, Fe)$_7$C$_3$ by *in situ* transformation. As the tempering is continued, (Cr, Fe)$_{23}$C$_6$ precipitates on grain boundaries and on subgrain boundaries, and grows massive by dissolving (Cr, Fe)$_7$C$_3$ within the grain.

2. Relation of precipitation process to variation in strength during tempering

Variation in Vickers hardness and 0.2% proof stress during tempering for various hours at 550°C were correlated with the change in structure. Fig. 2 shows the variations of hardness and 0.2% proof stress on tempering at 550°C correlated to the range of each carbide to exist, which was determined by electron diffraction pattern. (In Fig. 2, micro Vickers hardness was determined on thin sheets used in electron microscopy.) As shown in Fig. 2, the first softening occurs with the precipitation of Fe$_3$C, then the secondary hardening continues followed by the second softening in the stage of the transformation of Fe$_3$C into (Cr, Fe)$_7$C$_3$, and finally, (Cr,Fe)$_{23}$C$_6$ precipitates with slight softening.

(3) K. Kuo, J. Iron Steel Inst., **173** (1953), 363.
(4) E. Smith and J. Nutting, ibid., **187** (1957), 314.
(5) K.J. Irvine et al., J. Iron Steel Inst., **195** (1960), 386.
(6) T.M.F. Ronald and C. Bodsworth, ibid., **203** (1965), 252.
(7) A.K. Seal and R.W. Honeycomb, ibid., **188** (1958), 9.
(8) F.B. Pickering, I.S.I. Spec. Rept., No. 64 (1959), 23.
(9) V.P. Gupta and P.R. Dahr, J. Iron Steel Inst., **201** (1963), 213.
(10) K.C. Mills and A.G. Quarrell, ibid., **197** (1961), 9.
(11) V.B. Nileshwar and A.G. Quallel, I.S.I. Spec. Rept., No. 64 (1959), 259.
(12) J. Beech and D.H. Warrington, J. Iron Steel Inst., **204** (1966), 460.

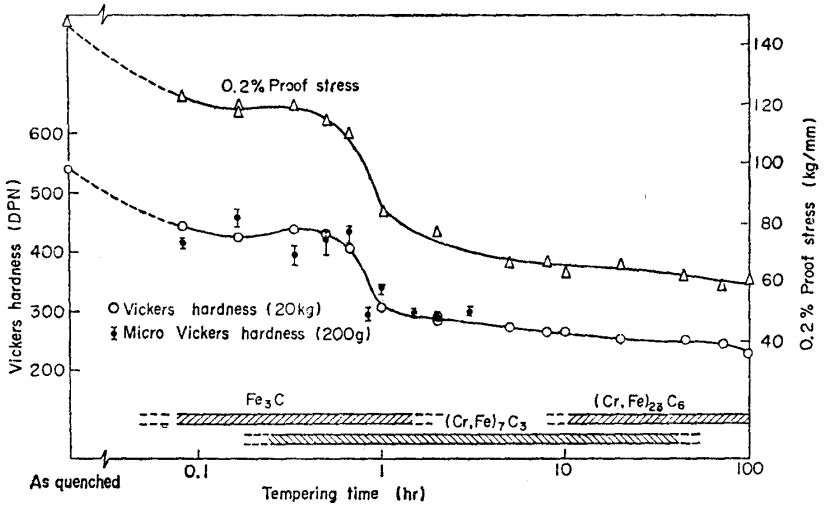

Fig. 2. Variations in hardness and 0.2% proof stress correlated with precipitation process during isothermal tempering at 550°C.

If it is assumed that the contributions of each strengthening factor to the yield strength of martensite are additive, σ_y is given as follows:

$$\sigma_y = \sigma_0 + f(\lambda) + \varphi(d) + \xi(\rho) + \phi_1(C_I) + \phi_1(C_s)$$

where σ_0 is yield strength of pure iron single crystal, $f(\lambda)$ the function of inter-particle distance λ, φ(d) the function of crystal diameter d, $\xi(\rho)$ the function of dislocation density ρ, $\phi(C_I)$ the function of concentration of interstitial atom C_I, and $\phi_2(C_s)$ the function of concentration of substitutional atom C_s.

On the other hand, the contributions of the above factors have been considered to change with tempering.[13)~15)] When the change of each factor is referred to tempering in the above equation, it is considered as follows: The grain size increases after tempering for more than 10 hr and changes scarcely within 10 hr as confirmed in the present case. (Quenched martensite is regarded as the group of small grains.) The dislocation density shows a trend to decrease with the tempering for 30 min to 2 hr, and especially after tempering for about 1 hr, the dislocations in the grain mostly disappear. On the other hand C, and Cr contents decrease with precipitation of carbides. With respect to the above, the following course can be considered as reasonable on the basis of the works by Sato et al. (on 0.37C–13Cr steel)[16] and by Fujita et al. (on 0.2%C-12%Cr-1%Mo steel)[17]: Solute carbon content decreases abruptly with the initial nucleation of Fe_3C, and then decreases gradually. On the other hand, solute chromium content decreases with

(13) A.R. Cox, J. Iron Steel Inst., **205** (1967), 55, 203.
(14) A.R. Cox, Proc. Internat. Conf. on the Strength of Metals and Alloys, Tokyo, (1967), 118.
(15) K. Monma et al., J. Japan Inst. Metals, **32** (1968), 143.
(16) T. Sato et al., J. Iron Steel Inst. Japan, **45** (1959), 816.
(17) Fujita et al., ibid., **46** (1960), 1395.

the nucleation of $(Cr, Fe)_7C_3$, taking an abrupt decrease with the precipitation of $(Cr, Fe)_{23}C_6$ after tempering for more than 10 hr. But the maximum decrease in chromium is calculated to be only 2%, even on the supposition of all carbon content forming $(Cr, Fe)_{23}C_6$. As the solid solution hardening by chromium is very small[18], the softening with decrease in chromium content can fairly be ignored.

From these points, it is considered probable that the first softening is due to the softening in matrix caused by decrease in solute content accompanied with precipitation rather than the hardening by Fe_3C precipitation. Secondary hardening observed in tempering for 20 to 30 min can not be explained by either grain size, dislocation density, or solid solution hardening, since the contributions of these factors decrease with tempering. Therefore, the precipitation hardening is considered to be the main factor.

In the past, such phenomena as precipitation[6] of $(Cr, Fe)_7C_3$ carbides, precipitation[5] of M_2X type nitrides and decomposition of residual austenite[19] are considered to be main causes for the secondary hardening in 12% Cr steel. In the present case, nitrogen content being 0.004%, precipitation hardening by nitrides is considered to be quite negligible. The decomposition of residual austenite in quenched specimen cannot be considered to be a main cause of secondary hardening, because volume percentage of residual austenite is estimated to be negligible by dilatation and structure observations. Therefore, granular $(Cr, Fe)_7C_3$ forming by separate nucleation on the dislocations in the region of high dislcoation density contributes greatly to the strength. Second softening which appears after 40 min in tempering is considered to be caused by abrupt decrease in dislocation density as well as by coagulation of precipitates.

3. Orientation relationships between precipitation carbide and matrix

By means of stereographic analysis of electron diffraction patterns, orientation relationships were determined between matrix and each of Fe_3C (orthorhombic $a_0=4.523$Å, $b_0=5.088$Å, $c_0=6.742$Å)[20], $(Cr, Fe)_7C_3$ (hexagonal $a_0=13.98$Å, $c_0=4.52$ Å)[20], and $(Cr, Fe)_{23}C_6$ (complex face centered cubic $a_0=10.64$Å)[20], all of which precipitated during tempering at 550°C.

Photo. 5(a) shows the diffraction pattern taken from the area where needle-like precipitates nucleate in the specimen tempered at 550°C for 1 hr, and 5(b) is its key diagram. The result of analysis made clear that this pattern consisted of (120) plane reflection of ferrite matrix and $(1\bar{1}0)$ plane reflection of Fe_3C. Therefore, the orientation relationships between them are as follows:

$$(001)_{FeC} \,//\, (2\bar{1}1)_{\alpha}$$

(18) G.E. Lacy and M. Gensamer, Trans. ASM, **32** (1944), 82.
(19) E.C. Bain, *The Alloying Elements in Steel*, A.S.M., (1952), 105.
(20) After A.S.T.M. cards.

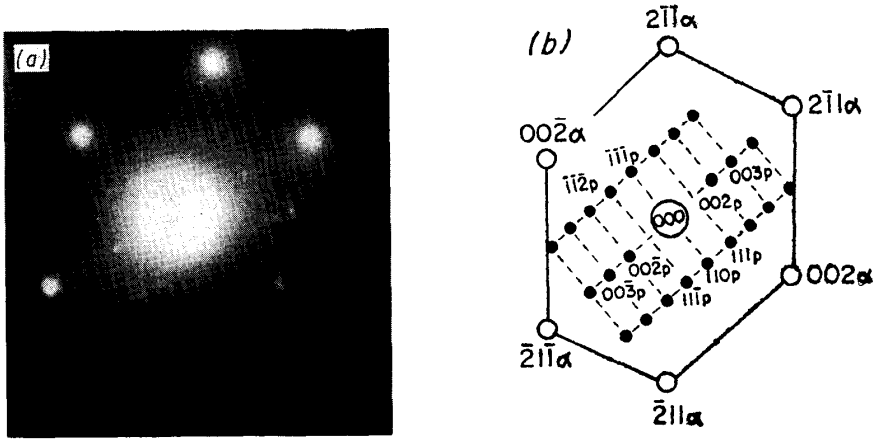

Photo. 5. (a) Electron diffraction pattern from a needle of Fe_3C in specimen tempered at 550°C for 1 hr.
(b) Key diagram of (a) pattern; ○ ferrite matrix, ● Fe_3C, incident beam // $[120]_\alpha$.

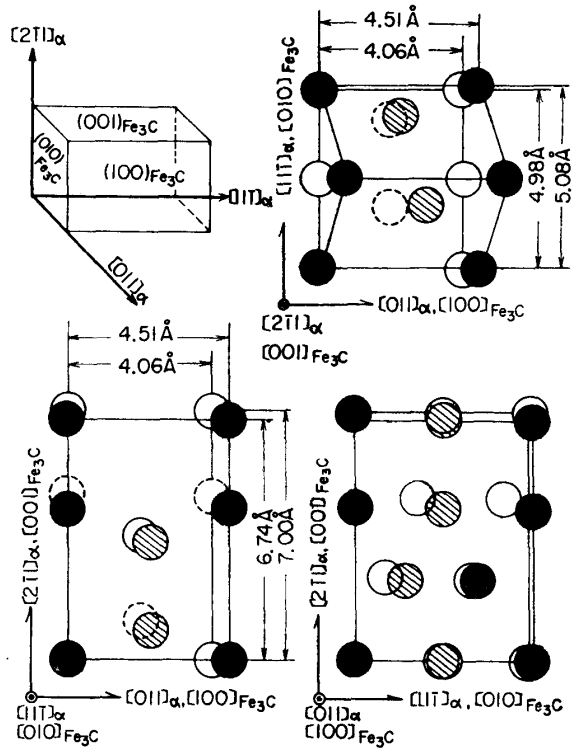

○ : Metal atom in ferite
◌ : Metal atom on plane of nearest neighbour in ferite
● : Metal atom in Fe_3C
◍ : Metal atom on plane of nearest neighbour in Fe_3C

Fig. 3. Relationship between positions of metal atoms in ferrite and Fe_3C

$$[100]_{Fe_3C} \,//\, [011]_\alpha$$

$$[010]_{FeC} \,//\, [111]_\alpha$$

These results are in good agreement with those in tempered or isothermally

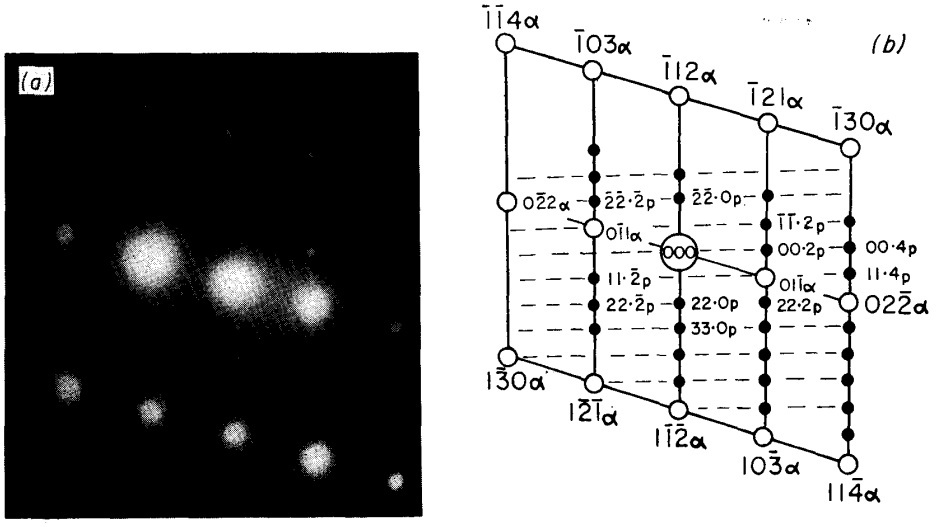

Photo. 6. (a) Electron diffraction pattern from a granular $(Cr, Fe)_7C_3$ in specimen tempered at 550°C for 8 hr.
(b) Key diagram of (a) pattern, ○ ferrite matrix, ● $(Cr, Fe)_7C_3$, incident beam // $(311)_\alpha$.

transformed carbon steel.[21]~[23] Fig. 3 shows relationships between positions of metal atoms in ferrite and Fe_3C according to the above relationships. Comparing the positions of metal atoms in Fe_3C with those in ferrite, it is made clear that metal atoms in ferrite are expanded by 2.6% in $[11\bar{1}]_\alpha$ direction, by 12% in $[011]_\alpha$ direction, and constricted by 3.7% in $(2\bar{1}1)_\alpha$ direction, that is, in the arrangement of Fe_3C lattice from ferrite, the $(011)_\alpha$ plane vertical to the $[011]_\alpha$ direction is most coherent to the metal atoms in Fe_3C. Therefore, it is reasonable that $(011)_\alpha$ plane becomes the habit plane of Fe_3C.

Photo. 6(a) shows the diffraction pattern taken from the area where granular carbides nucleate in the specimen tempered at 550°C for 8 hr and 6(b) its key diagram. As the result of analysis, this pattern is confirmed to consist of $[311]_\alpha$ zone axis and $[1\bar{1}00]_{(Cr,Fe)_7C_3}$ zone axis. Accordingly, the orientation relationships between them are settled as follows:

$$(0001)_{(Cr,Fe)_7C_3} \,//\, (\bar{1}7\bar{4})_\alpha$$

$$[11\bar{2}0]_{(Cr,Fe)_7C_3} \,//\, [1\bar{1}\bar{2}]_\alpha$$

$$[1\bar{1}00]_{(Cr,Fe)_7C_3} \,//\, [311]_\alpha$$

Though the unit cell of this $(Cr, Fe)_7C_3$ carbide is hexagonal, the coherency between atom arrangement in lattice and ferrite atoms could not be confirmed because of the unknown position of its atoms. But it has been found that diffraction pattern of $(1\bar{1}00)_{(Cr,Fe)_7C_3}$ reflection is in good agreement with that of

(21) W. Pitch, Arch. Eisenhütt., **34** (1963), 641.
(22) M.G.H. Wells, Acta Met., **12** (1964), 389.
(23) E. Tekin and P.M. Kelly, *Symposium on Precipitation from Iron Base Alloys*, Cleveland, U.S.A., 1963.

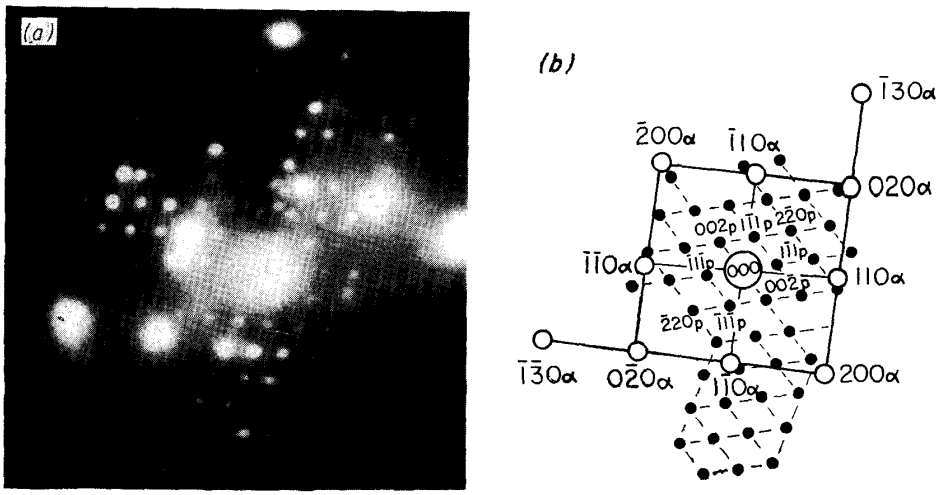

Photo. 7. (a) Electron diffraction pattern from a massive (Cr, Fe)$_{23}C_6$ in specimen tempered at 550°C for 100 hr.
(b) Key diagram of (a) pattern; ○ ferrite matrix, ● (Cr, Fe)$_{23}C_6$, incident beam // $[001]_\alpha$.

Table 2. Summaries of the precipitation characteristics of each carbides

Precipitate / Characteristics	Fe_3C	$(Cr,Fe)_7C_3$	$(Cr,Fe)_{23}C_6$
Orientation relationship	$(001)_{Fe_3C}$ // $(2\bar{1}1)_\alpha$ $[100]_{Fe_3C}$ // $[011]_\alpha$ $[010]_{Fe_3C}$ // $[11\bar{1}]_\alpha$	$(0001)_{Cr_7C_3}$ // $(\bar{1}7\bar{4})_\alpha$ $[11\bar{2}0]_{Cr_7C_3}$ // $[1\bar{1}\bar{2}]_\alpha$ $[1\bar{1}00]_{Cr_7C_3}$ // $[311]_\alpha$	$(110)_{Cr_{23}C_6}$ // $(001)_\alpha$ $[001]_{Cr_{23}C_6}$ // $[100]_\alpha$ $[1\bar{1}0]_{Cr_{23}C_3}$ // $[010]_\alpha$
Habit plane	$\{110\}_\alpha$	—	—
Growth direction	$\langle 110\rangle_\alpha$	Partially $\langle 110\rangle_\alpha$	—
Precipitation site	Homogeneous precipitation within grain (regardless of dislocation structure)	Homogeneous precipitation within grain (a part of precipitates by *in situ* transformation, the other by separate nucleation	Mainly, heterogeneous precipitation at grain boundaries by separate nucleation
Shape	Needle-like	Granular or rod-like	Massive

$(010)_{Fe_3C}$ reflection, if the forbidden reflection conditions[24] is neglected. Then, the orientation relationships between them are

$$(100)_{Fe_3C} \,//\, (0001)_{(Cr,Fe)_7C_3}$$

$$[001]_{FeC} \,//\, [2\bar{1}\bar{1}0]_{(Cr,Fe)_7C_3}$$

$$[010]_{Fe_3C} \,//\, [01\bar{1}0]_{(Cr,Fe)_7C_3}$$

(24) *International Tables for X-ray Crystallography*, The Internat. Union of Crystallogr., (1952).

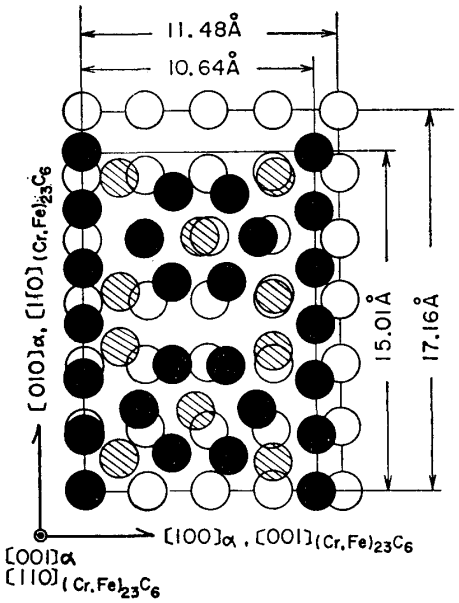

○ : Metal atom in ferrite ● : Metal atom in $(Cr, Fe)_{23}C_6$ ◍ : Metal atom on plane of nearest neighbour in $(Cr, Fe)_{23}C_6$

Fig. 4. Arrangement of metal atoms on the $(001)_\alpha$ and $(110)_{(Cr,Fe)_{23}C_6}$ planes.

That is, the length of a axis of Fe_3C (4.523Å) is consistent with that of c axis of (Cr, Fe)$_7C_3$ (4.523Å), and the length of c axis of Fe_3C (6.742Å) nearly equals half the length of a axis of (Cr,Fe)$_7C_3$(6.99Å), and five times the length of b axis of Fe_3C (25.44Å) almost equals twice the length of lattice distance of $(01\bar{1}0)_{(Cr,Fe)_7C_3}$ (24.22Å). These results suggest that Fe_3C into (Cr, Fe)$_7C_3$ transformation by *in situ* nucleation is possible.

Photo. 7(a) shows the diffraction pattern taken from the area where massive carbides nucleate in the specimen tempered at 550°C for 100 hr, and 7 (b) its key diagram. The analysis shows that the precipitate is (Cr, Fe)$_{23}C_6$, and in 7(b), the diffraction pattern consists of $(001)_\alpha$ plane reflection and $(1\bar{1}0)_{(Cr,Fe)_{23}C_6}$ plane reflection. Therefore, orientation relationships between ferrite matrix and (Cr, Fe)$_{23}C_6$ are as follows:

$$(110)_{(Cr,Fe)_{23}C_6} \;//\; (001)_\alpha$$

$$[001]_{(Cr,Fe)_{23}C_6} \;//\; [100]_\alpha$$

$$[1\bar{1}0]_{(Cr,Fe)_{23}C_6} \;//\; [010]_\alpha$$

Fig. 4 shows the arrangement of metal atoms on the $(001)_\alpha$ and the $(110)_{(Cr,Fe)_{23}C_6}$ plane based on the above relationships. When the positions of metal atoms in (Cr, Fe)$_{23}C_6$ are related to those in ferrite, the former are constricted by about 14% in $[010]_\alpha$ direction on one hand, and expanded by 7.3% in $[100]_\alpha$ direction on the other. Therefore, it is supposed that the coherency between carbide and ferrite in this instance is very little.

Summary

Precipitation characteristics of 12% Cr steel during isothermal tempering were studied mainly by transmission microscopy and diffraction, and shape, nucleation site and habit plane of each carbide of (Fe_3C, $(Cr, Fe)_7C_3$, $(Cr, Fe)_{23}C_6$), and the orientation relationships between carbides and ferrite matrix were clarified. Furthermore, relations between secondary hardening and structure were examined. The results obtained may be summarized as follows:

(1) The shape, nucleation site and habit plane of each carbide of (Fe_3C, $(Cr, Fe)_7C_3$, $(Cr, Fe)_{23}C_6$), and the orientation relationships between carbides and ferrite matrix were clarified as shown in Table 2.

(2) The secondary hardening during tempering is reasonably caused by the granular carbides of $(Cr, Fe)_7C_3$ which are formed by separate nucleation on the dislocation in the region of high dislocation density.

(3) From the relations between carbides (especially Fe_3C, and $(Cr, Fe)_{23}C_6$) and ferrite matrix, and from the coherency between their structures, the coherency between carbide and ferrite is supposed to be very little.